Observation of Discrete Conventional Caroli–de Gennes–Matricon States in the Vortex Core of Single-Layer $FeSe/SrTiO_3$

Chen Chen,[1,4,*] Qin Liu,[1,2,4,*] Wei-Cheng Bao,[3,6,*] Yajun Yan,[1,4] Qiang-Hua Wang,[3,4,†] Tong Zhang,[1,4,‡] and Donglai Feng[1,4,5,§]

[1]State Key Laboratory of Surface Physics, Department of Physics, and Advanced Materials Laboratory, Fudan University, Shanghai 200438, China
[2]Science and Technology on Surface Physics and Chemistry Laboratory, Mianyang, Sichuan 621908, China
[3]National Laboratory of Solid State Microstructures & School of Physics, Nanjing University, Nanjing, 210093, China
[4]Collaborative Innovation Center of Advanced Microstructures, Nanjing 210093, China
[5]Hefei National Laboratory for Physical Science at Microscale and Department of Physics, University of Science and Technology of China, Hefei, Anhui 230026, China
[6]Zhejiang University of Water Resources and Electric Power, Hangzhou 310018, China

(Received 7 May 2019; revised manuscript received 9 February 2020; accepted 12 February 2020; published 6 March 2020)

Using low-temperature scanning tunneling microscopy (STM), we studied the vortex states of single-layer FeSe film on a $SrTiO_3$ (100) substrate, and the local behaviors of superconductivity at sample boundaries. We clearly observed multiple discrete Caroli–de Gennes–Matricon states in the vortex core, and quantitative analysis shows their energies well follow the formula: $E = \mu\Delta^2/E_F$, where μ is a half integer ($\pm 1/2, \pm 3/2, \pm 5/2\ldots$) and Δ is the mean superconducting gap over the Fermi surface. Meanwhile, a fully gapped spectrum without states near zero bias is observed at the $[110]_{Fe}$ oriented boundary of 1 and 2 ML FeSe films, and atomic step edge of 1 ML FeSe. Accompanied with theoretical calculations, our results indicate an s-wave pairing without sign change in the high-T_C $FeSe/SrTiO_3$ superconductor.

DOI: 10.1103/PhysRevLett.124.097001

In superconductors, localized quasiparticle states at the boundaries such as magnetic vortices and superconducting or nonsuperconducting (S-N) interfaces, can provide critical information on electron pairing. As for conventional s-wave superconductor, there are so-called Caroli–de Gennes–Matricon (CdGM) states in the vortex cores [1] with $E = \mu\Delta^2/E_F$, where μ is a *half* integer ($\pm 1/2, \pm 3/2\ldots$); while for superconductors with sign-changing order parameter, such as d wave and p wave, the vortex states have qualitatively different energy characteristic [2] (e.g., $E = 0$ state is expected for chiral p-wave superconductor). However, in practice, the identification of CdGM states has long been hampered by their small energy spacing ($\delta E \sim \Delta^2/E_F$), which is in the μeV range for conventional low-T_C superconductors [3–4]. Progresses are only achieved recently in the iron-based superconductor Fe(Te, Se) [5–7] and (Li,Fe)OHFeSe [8,9], in which discrete vortex states accompanied by a zero-bias conductance peak (ZBCP) were observed. In particular, quantized conductance of the ZBCP has been observed in (Li,Fe)OHFeSe [9], indicating its topological nature and the presence of Majorana zero mode. Meanwhile, zero-energy or dispersive Andreev bound states (ABS) at S-N boundaries are expected for certain sign-change (e.g., d wave [10]) or topological superconductors [11], but not for s-wave superconductors. Nonetheless the detection of ABS relies on clean S-N boundaries and well resolved gap spectrum, which are nontrivial in practice.

Single-layer FeSe on $SrTiO_3$ probably has the highest T_C ($\geq$65 K) among all the Fe-based superconductors [12–19]. Its pairing symmetry is thus of great importance [20]. Previous STM study has suggested a plain s-wave pairing from impurity effect and quasiparticle interference (QPI) [18]. Nonetheless, a recent theoretical work shows that a nodeless d-wave pairing is possible if there is band hybridization induced by small spin-orbit coupling (SOC) [21]. Moreover, since calculations did not show topological band structure near the Fermi level of single-layer $FeSe/SrTiO_3$ [22], it thus serves as an important counterpart of the topologically nontrivial Fe(Se,Te) [6,7,23,24] and (Li,Fe)OHFeSe [8]. Examining the vortex states of $FeSe/SrTiO_3$ would provide information on both the pairing symmetry and factors for the presence or absence of Majorana zero mode.

Here we report a low-temperature STM study on the vortex states and S-N boundaries of single-layer $FeSe/SrTiO_3(100)$. We observed multiple discrete CdGM states with energies of $E = \mu(\delta E)$, where μ is a half integer and $\delta E = \Delta^2/E_F$. Quantitatively, δE can be accounted by an anisotropic superconducting gap with a mean size of Δ_0, which also explains the double coherence peaks in the tunneling spectrum. Our detailed model calculation shows the observed CdGM states agree with plain s wave but disfavors d-wave pairing, which is further supported by observation of full superconducting gap at both $[110]_{Fe}$

oriented 1 to 2 ML FeSe boundary and 1 ML FeSe step edge. Our results provide critical information on the pairing in this remarkable interfacial superconductor, and suggest the importance of out-of-plane coupling in realizing topological superconductivity in iron-based superconductors.

The FeSe films were grown by co-evaporating selenium (99.999%) and iron (99.995%) (flux ratio ~10:1) on Nb(0.5%) doped $SrTiO_3(001)$ substrate at 400 °C and postannealed at 500 °C to improve crystallinity. STM measurement was conducted in a cryogenic STM (UNISOKU) with a base temperature of $T = 0.4$ K and an electron temperature (T_{elec}) of 1.18 K (see part I of the Supplemental Material [25]). Pt/Ir tips were used after treatment on the Au(111) surface. dI/dV spectra were obtained by the standard lock-in technique with $f = 714$ Hz.

Figure 1(a) shows a typical topography of $FeSe/SrTiO_3$ with nominal thickness of 1.3 ML, and Fig. 1(b) is a zoomed image of 1 ML FeSe region. The tunneling spectra taken on defect-free area displays a full superconducting gap with a flat bottom and two pairs of coherence peaks [Fig. 1(c)]. Under a vertical magnetic field of $B = 10$ T, vortices show up in the zero-bias dI/dV mapping [Fig. 1(d)]. Some of the vortices are pinned by surface defects which can induce a strong in-gap state (Fig. S3 [25]), as indicated by arrows in Figs. 1(b) and 1(d); while the ones marked by circles display clean local superconducting gap at zero field and we refer them as "free" vortices (see part II of the Supplemental Material [25] for detailed gap measurement of free vortices regions). The superconducting coherence length (ξ) extracted from vortex mapping is 2.03–2.45 nm (Fig. S4 [25]), which is significantly smaller than averaged intervortex spacing at $B = 10$ T (~15.5 nm), therefore any intervortex coupling is expected to be weak here (see part III of the Supplemental Material [25] for more discussions, which includes Ref. [26]). Below we will focus our study on free vortex cores.

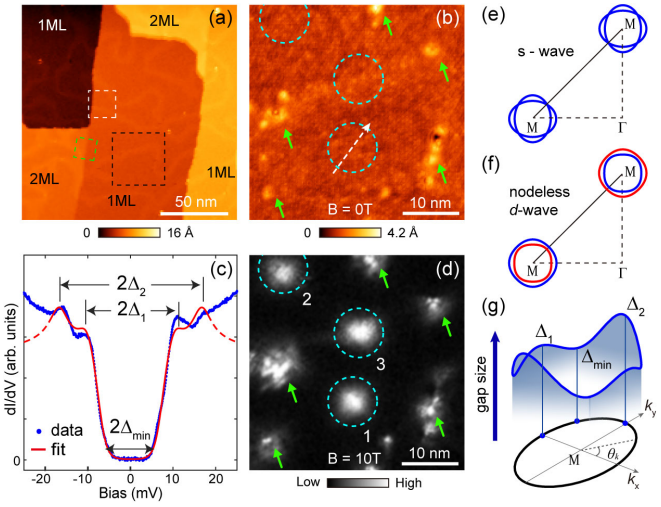

FIG. 1. (a) STM image of $FeSe/SrTiO_3$ film with a thickness of ~1.3 ML (160×160 nm^2, $V_b = 3$ V, $I = 5$ pA). (b) Image of a 1 ML region (40×40 nm^2) (c) Averaged gap spectrum of 1 ML FeSe ($V_b = 30$ mV, $I = 60$ pA, T = 4.2 K), taken along the white arrow in (b) at $B = 0$ T, and the gap fitting using Eq. (1). (d) Zero-bias dI/dV mapping taken on the same area of (b), at $B = 10$ T. Green arrows in (b) and (d) indicate surface defects and the pinned vortices, dashed circles indicate free vortices. (e) and (f) Sketch of Fermi surface of 1 ML FeSe in the folded BZ with $s_{(++)}$ wave and nodeless d-wave pairing, respectively. (g) Sketch of the gap distribution on the electron pocket at M [determined by Eq. (1)]. Δ_2, Δ_1, and Δ_{min} correspond to the two local gap maxima and the gap minima, respectively, and $tg(\theta_k) = k_y/k_x$.

As the double-gapped superconducting spectrum was commonly observed [12,18], we shall examine its origin. For single-layer $FeSe/SrTiO_3$, there are two electron pockets on each M point in the folded Brillouin zone (BZ) [Fig. 1(e)], and there could be finite band hybridization between them [Fig. 1(f), on which the nodeless d-wave pairing relies [21]]. So far various ARPES studies have discovered significant gap anisotropy on a *single* electron pocket, however hybridizations have not been observed within the experimental resolution [17,19]. Here we find that the ARPES measured anisotropic gap function in Ref. [19],

$$\Delta_k = \Delta_0 - A\cos(2\theta_k) + B\cos(4\theta_k), \tag{1}$$

spectrum. As illustrated in Fig. 1(g), such a gap function produces two local gap maxima of Δ_2 ($=\Delta_0 + A + B$) at $\theta_k = \pi/2$, and $3\pi/2$, and Δ_1 ($=\Delta_0 - A + B$) at $\theta_k = 0$, and π, which generate two pairs of coherence peaks in dI/dV; while Δ_0 is the mean gap over the Fermi surface. The corresponding fit in Fig. 1(c) yields $\Delta_0 = 10.58$, $A = 3.25$, and $B = 2.87$ meV. Details of the fitting procedure are described in part IV of the Supplemental Material [25].

Figure 2 presents the tunneling spectra of four different free vortices, obtained at $T = 0.4$ K ($T_{elec} = 1.18$ K). Figure 2(a) shows the dI/dV line cut taken across vortex 1, with clear multiple discrete peaks near the core center. These peaks locate symmetrically with respect to E_F, but *no* ZBCP is observed. Figure 2(e) shows the spatial evolution of the spectra in a color plot. Discrete states can be seen within a ± 2 nm range around the center and vanish outside; meanwhile, a pair of broader peaks shows up at higher energies [shaded regions in Fig. 2(a)]. Those broader peaks keep moving to high energy and eventually merge into the coherence peaks. Similar behaviors were observed on other free vortices [see Fig. 2(b) for vortex 2 and Fig. S6 of Ref. [25] for vortices 3,4).

To better resolve the low-energy core states, Figs. 2(c) and 2(d) show the dI/dV focusing on small energy scale (± 6 meV), taken at the cores of vortices 3 and 4. Clearly, there are up to six well-separated peaks symmetrically distributed with respect to E_F. Those peaks are equally spaced and their positions almost keep the same within

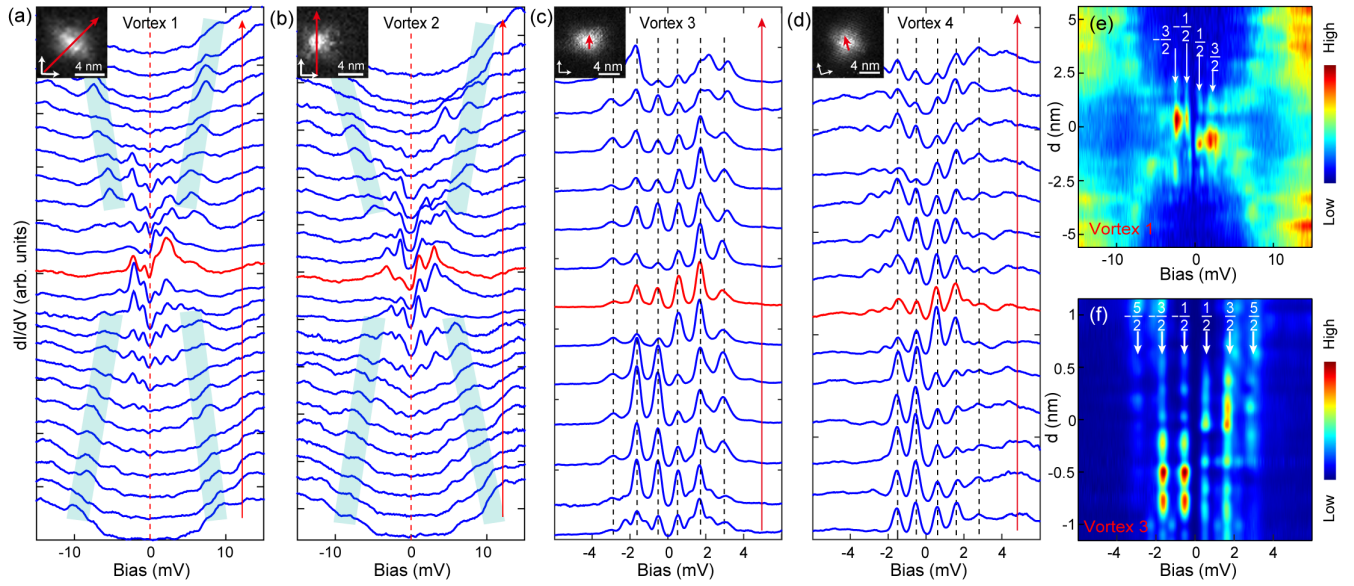

FIG. 2. Discrete bound states in free vortices. (a)–(b) dI/dV spectra taken across vortex 1 and 2 ($V_b = 20$ mV, $I = 60$ pA, $\Delta V = 0.1$ mV). (c)–(d) dI/dV spectra taken in small energy range across the center of vortices 3 and 4 ($V_b = 6$ mV, $I = 60$ pA, $\Delta V = 0.1$ mV). Red curves in (a)–(d) are collected at the vortex center (estimated), and insets are vortex maps. (e)–(f) Color plot of the spectra in (a) and (c), respectively. Arrows indicate the individual CdGM states. All the spectra are taken at $T = 0.4$ K ($T_{\text{elec}} = 1.18$ K)

± 1.2 nm around the core. A color plot of Fig. 2(c) is shown in Fig. 2(f).

We applied multiple-Gaussians fitting to the summed spectra near the center of vortices 1–4, as shown in Figs. 3(a)–3(d). The fitted peak energies are labeled, and detailed fitting parameters including the peak width and fitting errors are presented in part VI of Supplemental Material [25]. Figure 3(e) shows the normalized peak energies of vortices 1–4 by dividing with their averaged spacing (δE). The results sit well on the lines of *half* integer value ($\pm 1/2$, $\pm 3/2$, or $\pm 5/2$), which is expected for the CdGM states of an s-wave superconductor. Moreover, the high-energy shifting peaks are expected to be closely packed states, as the spacing of CdGM states decreases at high energy; and their maximal intensity locations move away from the core center [4]. Therefore, we resolved both discrete low-energy states and quasicontinuous high-energy states in single-layer FeSe, for its large gap, small E_F, and high resolution here.

Nonetheless, the energy spacing δE varies from 1.1 to 1.9 meV for different vortices, which is likely due to superconducting gap variations. To have a quantitative analysis, we extracted the mean size (Δ_0) of the local gap where vortices 1–4 emerge (Fig. S2), by fitting them with the same way as discussed in part IV of the Supplemental Material [25]. We found that the δE of different vortices can be reasonably accounted by $(\Delta_0)^2/E_F$ (taking a constant $E_F = 60$ meV from our previous QPI study [18]). A linear fit of $(a\Delta_0)^2/E_F$ to δE yields $a = 0.95(\pm 0.14)$ [Fig. 3(f)]. Therefore, a single anisotropy gap can account for both

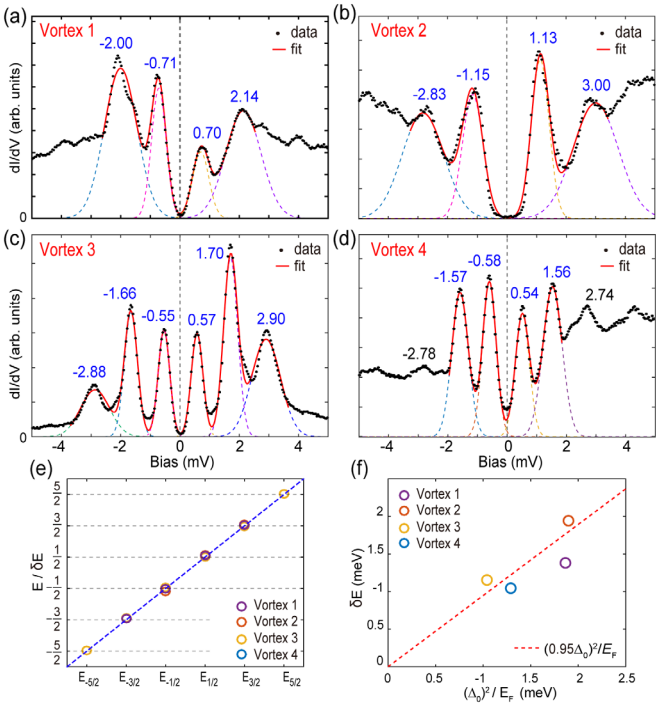

FIG. 3. Quantitative fitting of vortex bound states. (a)–(d) Low energy spectra of free vortices 1–4. Red curves are multiple Gaussian-peak fits (dashed curves are individual peaks). (e) Normalized energy of the CdGM state of vortices 1–4, via dividing the averaged δE of each vortex. (f) The relation of $(\Delta_0)^2/E_F$ and δE for vortices 1–4, dashed line is the linear fitting.

superconducting gap spectrum and the CdGM states, band hybridization is not necessarily involved here.

The behaviors of the CdGM states of single-layer FeSe/$SrTiO_3$ match those of an s-wave superconductor. The absence of ZBCP here excludes topological superconductivity as in Fe(Se,Te) [6,7] and (Li,Fe)OHFeSe [8,9], or chiral p-wave pairing. Nonetheless, a theoretical study suggests that a nodeless d-wave pairing is possible if the two electron pockets of FeSe/$SrTiO_3$ are hybridized by SOC [21], as sketched in Fig. 1(f). Since finite SOC has been widely observed in iron-based superconductors [27], and in particular ARPES study [19] sets the upper limit of the SOC of FeSe/$SrTiO_3$ to be 5 meV (limited by its resolution), we shall examine whether this scenario could explain our observation. We simulated the vortex states of 1 ML FeSe/$SrTiO_3$ based on a two-band $\boldsymbol{k}\cdot\boldsymbol{p}$ model that includes SOC and hybridization [21], under both s-wave and nodeless d-wave pairing. Details of the model are described in part VII of the Supplemental Material [25], and in which the parameters are chosen to mimic the experimentally measured Fermi surface and superconducting gap.

Figure 4(a) presents the simulation for plain s-wave pairing at zero SOC strength ($\lambda = 0$). It displays typical CdGM states that symmetrically distributed around E_F with equal spacing. As approaching the core center, the intensities of low level states increase and show certain particle-hole asymmetry [4]. These overall behaviors qualitatively agree with our data in Fig. 2 and Fig. S6. After applying SOC up to $\lambda = 0.03t$ ($\approx$4 meV, $t = 135$ meV is a model parameter), there is no obvious change in the simulated CdGM state, as demonstrated in Fig. 4(c) and Fig. S9 of Ref. [25]. This is because for s-wave pairing, SOC simply shifts the chemical potential of the two hybridized bands (to opposite direction), the resulting modification on the CdGM state ($E = \mu\Delta^2/(E_F \pm \lambda)$) is negligible when $\lambda \ll E_F$.

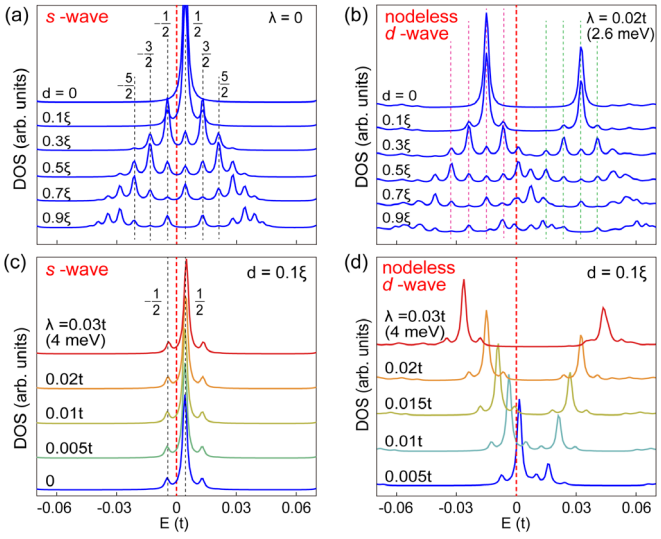

FIG. 4. Calculated vortex states under s-wave pairing (a) without SOC, and nodeless d-wave pairing (b) with $\lambda = 0.02t$, at different distance to the core center (ξ is the coherence length). Calculated vortex states under s-wave (c) and nodeless d-wave (d) pairing at $d = 0.1\xi$, with various SOC strength.

For nodeless d-wave pairing, finite SOC must be present to avoid band crossing [Fig. 1(f)]. Figure 4(b) shows the corresponding simulation with $\lambda = 0.02t$ ($\sim$2.7 meV). Noticeably, it displays *two* sets of CdGM states (from the two hybridized bands), with energies shifted to opposite directions. We further found such energy shift is of the similar amount of λ, as shown in Fig. 4(d). A simple understanding is that for a nodeless d-wave that relies on hybridization, the SOC acts as a shift of "chemical potential" for Bogoliubov–de Gennes (BdG) quasiparticles [21], which will directly shift vortex states as $E = (\mu\Delta^2/E_F) \pm \lambda$ (see part VII of the Supplemental Material [25] for more discussion). However, this contradicts our experimental observations of symmetrically distributed and equally spaced CdGM states within an uncertainty $\lesssim \pm 0.02$ meV (see Table S2 in Ref. [25]), despite the sizable variations of the gap and δE. In fact, any asymmetric offset or splitting larger than a fraction of our resolution (0.36 meV) would have been easily resolved by STS. As SOC is a necessary condition (and in Ref. [21] sizable SOC is needed to explain the ARPES observed gap anisotropy), our observation thus strongly disfavors nodeless d-wave pairing.

We note that despite the energy of CdGM states well agreeing with s-wave pairing, their intensities show some irregular distribution around the core center, as seen in Figs. 2(e) and 2(f). Further simulations (part VIII of the Supplemental Material [25]) show that this could be due to randomly distributed interfacial disorders in FeSe/$SrTiO_3$, which can locally affect the intensity of the CdGM state. We also note the Zeeman effect at $B = 10$ T is unlikely to affect the superconducting pairing here, since the Zeeman energy ($\sim$1.1 meV) is still significantly smaller than the gap of FeSe/$SrTiO_3$ ($\sim$10 meV).

To gain more information on the pairing, we examined the states at the boundaries of the FeSe/$SrTiO_3$ film. It was suggested that for a d_{x2-y2}-wave superconductor, zero-energy ABS would exist at the $\{[110]\}$ oriented boundaries due to the π-phase shift in the reflection of quasiparticles [10]; while topologically nontrivial superconductors possess dispersive ABS at all surface and edges, which give finite DOS within the superconducting gap [11]. However, usually ABS is not expected at the boundary of conventional s-wave superconductors.

In the FeSe film presented in Fig. 1(a), there are boundaries between 2 ML FeSe and 1 ML FeSe regions with *continues* surface lattice. The nonsuperconducting 2 ML FeSe [12] made such boundaries well-defined 1D S-N interfaces. Figure 5(a) shows such a boundary along $\boldsymbol{a_0}$, i.e., the [110] direction of the Fe lattice, where

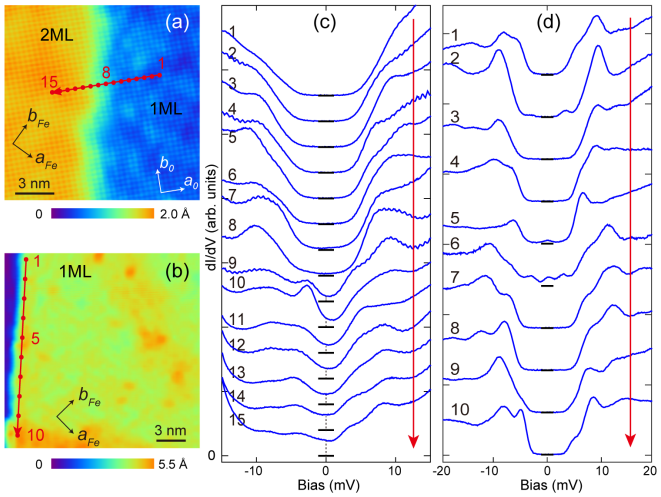

FIG. 5. STM images of a boundary between 2 ML/1 ML FeSe (a) and atomic step edge of 1 ML FeSe (b), taken within the green and white dashed square in Fig. 1(a), respectively. (c)–(d) dI/dV spectra taken along the arrow in panel (a) and (b), respectively ($T = 4.2$ K). The short black bars indicate the zero-conductance position of each curve.

zero-energy ABS is expected for d-wave pairing with sign-change between adjacent M points [Fig. 1(f)]. Figure 5(c) shows a dI/dV line cut taken across such a boundary, with a spatial interval of 0.6 nm [marked in Fig. 5(a)]. The gap of 1 ML FeSe, with flat and zero-DOS bottom, keeps untouched until very close to interface ($\leq$1 nm); then the gap quickly disappeared at the interface and shows a metallic DOS on the 2ML FeSe side. There is no ZBCP formed at both sides of the interface.

Figure 5(b) presents another type of boundary: the [110] oriented step edge of 1 ML FeSe. The dI/dV spectra taken along the edge, within a distance $\leq$1 nm, are shown in Fig. 5(d). The majority of the spectra show a full superconducting gap with flat bottom; while some spectra occasionally show irregular in-gap states (e.g., spectra 1, 2, 5, 6). Since a discontinuous step edge is more likely to have local disorders and defects, the fully gapped spectrum is likely the intrinsic feature on the step edge while the in-gap states are generated by local disorders. Overall, there is no zero-energy ABS or intrinsic in-gap states on both types of [110]-oriented boundaries, which disfavors d-wave or topologically nontrivial superconductors (e.g., chiral p wave), but is consistent with the plain s-wave pairing.

Our studies of CdGM states and boundary states provide independent evidences on the s-wave pairing in single-layer $FeSe/SrTiO_3$. This helps to clarify the current controversy on its pairing symmetry, and is consistent with the recently proposed cooperative pairing enhancement scenario [16,28]. Moreover, our results provide insight for the fast-developing field of topological superconductivity in iron-based superconductors. Interlayer coupling has been shown to create band inversion and topological surface states in Fe(Se,Te) [23,24] and (Li,Fe)OHFeSe [8], which eventually leads to possible Majorana zero modes. For $FeSe/SrTiO_3$, a 2D system, the absence of ZBCP in the vortex core and the absence of in-gap features at 1D boundaries in our data show that it is likely topologically trivial, although recent studies show that there is a SOC-induced gap below E_F at M points [22,29]. Therefore, our results further suggest that interlayer coupling is a prerequisite for topological superconductivity of iron-based superconductors.

We thank Professors Jiangping Hu and Yihua Wang for helpful discussions. This work is supported by the National Natural Science Foundation of China (Grants No. 11888101, No. 11790312, No. 11421404, and No. 11574134), National Key R&D Program of the MOST of China (Grants No. 2016YFA0300200, No. 2016YFA0300401, No. 2017YFA0303004), Science Challenge Project (Grant No. TZ2016004).

*These authors contributed equally to this work.
†Corresponding author.
qhwang@nju.edu.cn
‡Corresponding author.
tzhang18@fudan.edu.cn
§Corresponding author.
dlfeng@fudan.edu.cn

[1] C. Caroli, P. G. de Gennes, and J. Matricon, Bound Fermion states on a vortex line in a type II superconductor, J. Phys. Lett. **9**, 307 (1964).
[2] G. E. Volovik, Fermions on quantized vortices in superfluids and superconductors, Turk. J. Phys. **20**, 693 (1996).
[3] H. F. Hess, R. B. Robinson, R. C. Dynes, J. M. Valles, and J. V. Waszczak, Scanning-Tunneling-Microscope Observation of the Abrikosov Flux Lattice and the Density of States near and inside a Fluxoid, Phys. Rev. Lett. **62**, 214 (1989).
[4] N. Hayashi, T. Isoshima, M. Ichioka, and K. Machida, Low-Lying Quasiparticle Excitations Around a Vortex Core in Quantum Limit, Phys. Rev. Lett. **80**, 2921 (1998).
[5] M. Y. Chen, X. Chen, H. Yang, Z. Du, X. Zhu, E. Wang, and H.-H. Wen, Discrete energy levels of Caroli–de Gennes–Matricon states in quantum limit in $FeTe_{0.55}Se_{0.45}$, Nat. Commun. **9**, 970 (2018).
[6] D. F. Wang *et al.*, Evidence for Majorana bound state in an iron-based superconductor, Science **362**, 333 (2018).
[7] T. Machida, Y. Sun, S. Pyon, S. Takeda, Y. Kohsaka, T. Hanaguri, T. Sasagawa, and T. Tamegai, Zero-energy vortex bound state in the superconducting topological surface state of Fe(Se,Te), Nat. Mater. **18**, 811 (2019).
[8] Q. Liu *et al.*, Robust and Clean Majorana Zero Mode in the Vortex Core of High-Temperature Superconductor $(Li_{0.84}Fe_{0.16})$OHFeSe, Phys. Rev. X **8**, 041056 (2018).
[9] C. Chen, Q. Liu, T. Z. Zhang, D. Li, P. P. Shen, X. L. Dong, Z.-X. Zhao, T. Zhang, and D. L. Feng, Quantized conductance of Majorana zero mode in the vortex of the topological superconductor $(Li_{0.84}Fe_{0.16})$OHFeSe, Chin. Phys. Lett. **36**, 057403 (2019).

[10] K. Satoshi and T. Yukio, Tunnelling effects on surface bound states in unconventional superconductors, Rep. Prog. Phys. **63**, 1641 (2000).
[11] X. L. Qi and S. C. Zhang, Topological insulators and superconductors, Rev. Mod. Phys. **83**, 1057 (2011).
[12] Q. Y. Wang *et al.*, Interface induced high temperature superconductivity in single unit-cell FeSe films on $SrTiO_3$, Chin. Phys. Lett. **29**, 037402 (2012).
[13] D. F. Liu *et al.*, Electronic origin of high-temperature superconductivity in single-layer FeSe superconductor, Nat. Commun. **3**, 931 (2012).
[14] S. L. He *et al.*, Phase diagram and electronic indication of high-temperature superconductivity at 65K in single-layer FeSe films, Nat. Mater. **12**, 605 (2013).
[15] S. Y. Tan *et al.*, Interface-induced superconductivity and strain-dependent spin density waves in $FeSe/SrTiO_3$ thin films, Nat. Mater. **12**, 634 (2013).
[16] J. J. Lee *et al.*, Interfacial mode coupling as the origin of the enhancement of T_c in FeSe films on $SrTiO_3$, Nature (London) **515**, 245 (2014).
[17] R. Peng *et al.*, Measurement of an Enhanced Superconducting Phase and a Pronounced Anisotropy of the Energy Gap of a Strained FeSe Single Layer in $FeSe/Nb:SrTiO_3/KTaO_3$ Heterostructures Using Photoemission Spectroscopy, Phys. Rev. Lett. **112**, 107001 (2014).
[18] Q. Fan *et al.*, Plain s-wave superconductivity in single-layer FeSe on $SrTiO_3$ probed by scanning tunneling microscopy, Nat. Phys. **11**, 946 (2015).
[19] Y. Zhang, J. J. Lee, R. G. Moore, W. Li, M. Yi, M. Hashimoto, D. H. Lu, T. P. Devereaux, D.-H. Lee, and Z.-X. Shen, Superconducting Gap Anisotropy in Monolayer FeSe Thin Film, Phys. Rev. Lett. **117**, 117001 (2016).
[20] P. J. Hirschfeld, M. M. Korshunov, and I. I. Mazin, Gap symmetry and structure of Fe-based superconductors, Rep. Prog. Phys. **74**, 124508 (2011).
[21] D. F. Agterberg, T. Shishidou, J. O'Halloran, P. M. R. Brydon, and M. Weinert, Resilient Nodeless d-Wave Superconductivity in Monolayer FeSe, Phys. Rev. Lett. **119**, 267001 (2017).
[22] N. Hao and J. Hu, Topological Phase in the Single-Layer FeSe, Phys. Rev. X **4**, 031053 (2014).
[23] Z. Wang *et al.*, Topological nature of the $FeSe_{0.5}Te_{0.5}$ superconductor, Phys. Rev. B **92**, 115119 (2015).
[24] G. Xu, B. Lian, P. Tang, X.-L. Qi, and S.-C. Zhang, Topological Superconductivity on the Surface of Fe-Based Superconductors, Phys. Rev. Lett. **117**, 047001 (2016).
[25] See Supplemental Material at http://link.aps.org/supplemental/10.1103/PhysRevLett.124.097001 for additional data, method, and discussions.
[26] M. Cheng, R. M. Lutchyn, V. Galitski, and S. Das Sarma, Splitting of Majorana-Fermion Modes due to Intervortex Tunneling in a $px + ipy$ Superconductor, Phys. Rev. Lett. **103**, 107001 (2009).
[27] S. V. Borisenko *et al.*, Direct observation of spin–orbit coupling in iron-based superconductors, Nat. Phys. **12**, 311 (2016).
[28] Q. Song *et al.*, Evidence of cooperative effect on the enhanced superconducting transition temperature at the $FeSe/SrTiO_3$ interface, Nat. Commun. **10**, 758 (2019).
[29] Z. F. Wang *et al.*, Topological edge states in a high-temperature superconductor $FeSe/SrTiO_3(001)$ film, Nat. Mater. **15**, 968 (2016).